ELSEVIER

Journal of Alloys and Compounds 317–318 (2001) 274–279

Journal of ALLOYS AND COMPOUNDS

www.elsevier.com/locate/jallcom

Structure and magnetism in the polymorphous MnFeAs

Janusz Tobola[a,*], Madeleine Bacmann[b], Daniel Fruchart[b], Pierre Wolfers[b], Stanislaw Kaprzyk[a], Abdel-Azziz Koumina[c]

[a]*Faculty of Physics and Nuclear Techniques, AGH, 30-059 Kraków, Poland*
[b]*Laboratoire de Cristallographie, CNRS, BP 66, 38042 Grenoble Cedex 09, France*
[c]*Laboratoire de Chimie du Solide Minéral, Université Semlalia, BP 2390, Marrakech, Morocco*

Abstract

Two crystallographic phases of MnFeAs were stabilised: the tetragonal Fe_2As-type structure or the hexagonal Fe_2P-type one, if synthesis is performed under normal conditions, or high pressure and temperature. The structural, magnetic and electronic properties of both MnFeAs polytypes are investigated using magnetisation, neutron diffraction measurements as well as band structure calculations by the Korringa–Kohn–Rostoker method. The tetragonal phase is antiferromagnetic (T_N=470 K) with the magnetic cell doubled along *c*-axis, with respect to the chemical one. The local magnetic moment on Mn(2c) refined from neutron study is 3.36 μ_B, while no significant magnetic moment is observed on the Fe(2a) site. The hexagonal phase is ferromagnetic with T_C near 190 K. The magnetic moments determined by neutron diffraction are 3.14 and 1.54 μ_B on Mn(3g) and Fe(3f), respectively. Upon applying a magnetic field as large as 10 T the saturation magnetisation of 4.5 μ_B/f.u. is measured at 5 K. From non-polarised KKR calculations we deduce, that the Fermi level falls into a deep minimum of density of states (DOS) in the tetragonal as well as in the hexagonal variants of MnFeAs, which may tentatively explain the structural stability of both phases. The spin-polarised band structure study of the tetragonal MnFeAs (AFM) shows DOS splitting exclusively on the Mn(2c) sites, resulting in the local magnetic moment of 3.42 μ_B, unlike the hexagonal MnFeAs (FM) where the magnetic moments of 3.13 and 1.10 μ_B are found on Mn(3g) and Fe(3f), respectively. Moreover, the influence of lattice parameter variation on electronic and magnetic properties is discussed based on total energy KKR calculations.

Keywords: Iron manganese compounds; Neutron diffraction; Magnetisation; Band structure calculations; Total energy analysis; KKR method

1. Introduction

Peculiar magnetic and structural properties of the phosphide–arsenide MnFe(As–P) system have attracted attention over last two decades [1–5]. The parent MnFeAs compound belongs to the large and well-known MM′X (M, M′=transition elements and X=As, P) family of compounds, which generally crystallise in three related structures (*P*-62*m* – H, *P*4/*nmm* – T, *Pnma* – O). All these structures contain two common polyhedra, which form the coordination of metal atoms in tetrahedral (t) and square-pyramidal (p) sites [6]. Interestingly, two of the above-mentioned structures were observed in the MnFeAs system: the T (the Fe_2As-type) [7] or the H (the Fe_2P-type) structures, if synthesis of the sample is performed under normal conditions or high pressure and temperature (p=3.5 GPa, T=800°C) [8]. In both phases the Mn atoms occupy the pyramidal sites while the Fe atoms are located in the tetrahedra.

In the previous works [9,10], T-MnFeAs was found to be an antiferromagnet with a Neél temperature at 463 K, being near the mean value between T_N of Mn_2As (T_N= 573 K) and Fe_2As (T_N=325 K). Nevertheless, the magnetic moment on the (t) site in T-MnFeAs (0.2 μ_B on Fe(t) and 3.6 μ_B on Mn(p) [9,10]) was found to be rather small if compared to the respective values in Mn_2As, namely: 3.5 μ_B (t), 3.7 μ_B (p) [11] and 2.1 μ_B (t), 4.2 μ_B (p) [12] as well as in Fe_2As: 1.28 μ_B (t), 2.05 μ_B (p) [13]. The magnetic moments arrangement along the *c*-axis is described by the sequences: '+ - + - + -' (Mn_2As) and '+ + - - - +' (Fe_2As) for the succession 't p p t p p' of the tetrahedral pyramidal and sites.

In this paper we present investigations of the magnetic properties and electronic structure of the two crystallographic variants of MnFeAs, using neutron powder diffrac-

*Corresponding author. Tel.: +48-12-172-982; fax: +48-12-340-010.
E-mail address: tobola@ftj.agh.edu.pl (J. Tobola).

0925-8388/01/$ – see front matter
PII: S0925-8388(00)01347-5

Table 1
Cell and position parameters of the tetragonal and hexagonal types of MnFeAs

Tetragonal MnFeAs		
T (K)	5	233
a (Å)	3.7429(1)	3.7425(3)
c (Å)	5.9947(2)	6.0292(3)
Mn(2c): 0, 1/2, z	0.3293(4)	0.332(1)
As(2c): 0, 1/2, z	0.746(2)	0.744(1)
Fe(2a): 0, 0, 0		
Hexagonal MnFeAs		
T (K)	5	250
a (Å)	6.263(1)	6.24907(5)
c (Å)	3.5440(9)	3.60497(6)
Mn(3g): x, 0, 1/2	0.590(1)	0.593(2)
Fe(3f): x, 0, 0	0.2557(1)	0.2530(9)

tion and magnetisation measurements as well as the self-consistent band structure calculations performed by the Korringa–Kohn–Rostoker method [14,15].

2. Experimental and theoretical details

The neutron diffraction experiments were carried out using the D1B diffractometer installed at the High Flux Reactor (ILL, Grenoble, France) at 5 K$<T<$250 K and $\lambda=2.526$ Å, recording long exposure patterns at selected temperatures. Magnetic measurements on powder samples were performed using a magnetometer with magnetic fields of 0.1 and 10 T, in the temperature ranging from 5 to 300 K. The crystal and magnetic structures were refined by the MXD program [16] using integrated intensities determined from the ABFIT program [17].

The electronic structure of the two phases of MnFeAs were calculated by the spin-polarised self-consistent Korringa–Kohn–Rostoker method within the LSD framework (using the exchange-correlation potential of Barth–Hedin form [18]) and applying experimental crystal parameters as well as the magnetic structure types (ferromagnetic in H-MnFeAs and antiferromagnetic in T-MnFeAs with a magnetic unit cell doubled along *c*-axis). Total, site- and l-decomposed densities of states (DOS) as well as local

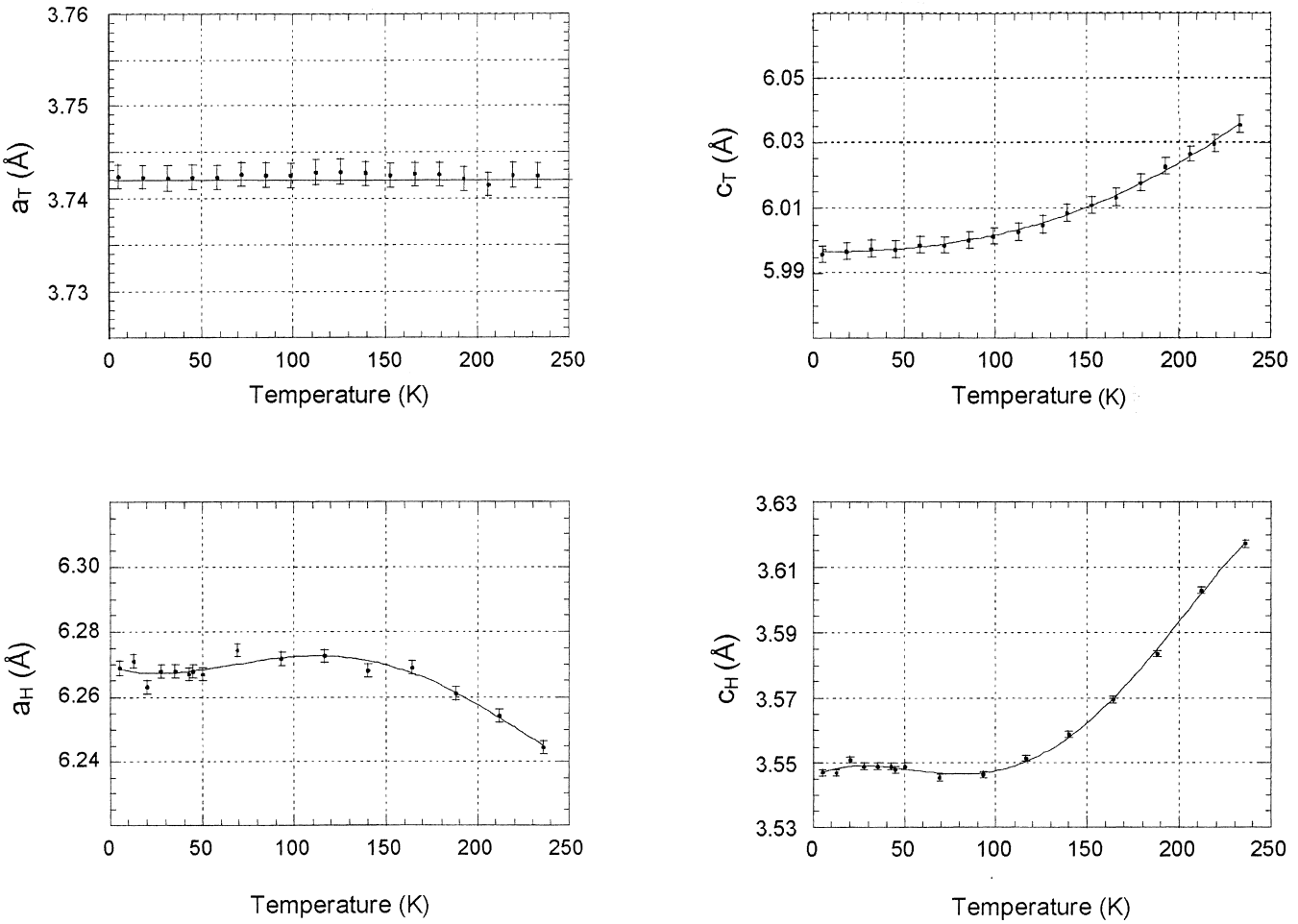

Fig. 1. Temperature dependence of the crystallographic lattice parameters in the tetragonal (a_T, c_T) and hexagonal (a_H, c_H) MnFeAs.

magnetic moments on inequivalent sites were computed for the final potentials converged up to 1*mRy*. Moreover, extensive total energy calculations were done varying the *a* and *c* lattice parameters (with atomic positions fixed), in order to obtain an insight in the structural and magnetic stability of MnFeAs.

3. Results and discussion

The structural parameters refined from neutron diffraction patterns are reported in Table 1. The analysis of the temperature dependent variations of *a* and *c* as well as a discussion concerning structural relations between the tetragonal and hexagonal polytypes was already presented in Ref. [8]. The H phase of MnFeAs obtained under pressure was found to have a reduced cell volume (about 5%) in respect to the T phase [8]. Interestingly, as seen from the temperature dependent lattice parameters shown in Fig. 1, at the low-temperature range the experimental a_T/c_T ratio in the T-MnFeAs compound is close to the c_H/a_H ratio found in H-MnFeAs but these factors vary in opposite directions with increasing temperature. The refinements of the neutron diffraction data revealed that the crystallographic ordering of Mn and Fe atoms is complete in both phases of MnFeAs, i.e., iron and manganese are located on tetrahedral and pyramidal sites, respectively. This is in agreement with a previous Mössbauer spectroscopy investigation [4]. Such a distribution of transition metal atoms in MnFeAs also agrees with the site selectivity rules established in the MM′X-type phosphides and arsenides: the larger atom prefers the pyramidal (larger) site, the more electropositive element needs the highest coordination number of p-site.

In Fig. 2 we present the non-polarised density of states (total as well as Mn and Fe-decomposed DOSs) in the two modifications of MnFeAs. In both cases the Fermi energy falls into deep minimum of the density of states. Thus $N_{tot}(E_F)=19.1$ st./Ry/spin per formula unit in T-MnFeAs, mostly due to $N_{Mn}(E_F)=11.3$ and $N_{Fe}(E_F)=6.4$, while the $N_{tot}(E_F)=22.3$ value was obtained for H-MnFeAs attributed mainly to transition metal sites, namely $N_{Mn}(E_F)=13.1$ and $N_{Fe}(E_F)=8.3$. It is worth noting that the conduction band is found to be slightly broadened in H-MnFeAs in comparison to T-MnFeAs and this effect can be related to the smaller volume of unit cell of the hexagonal sample.

The band energy contribution to the total energy of the

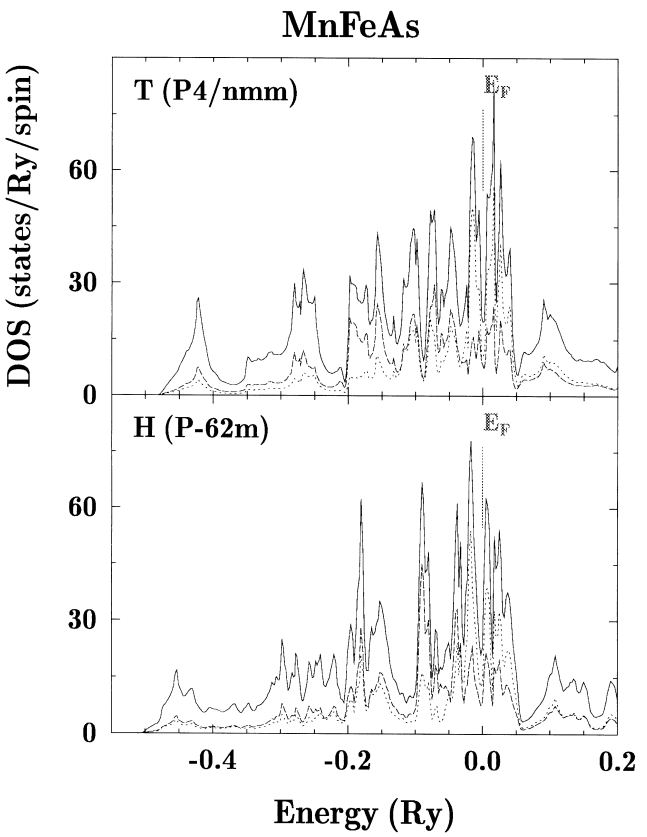

Fig. 2. Non-polarised KKR DOS in the tetragonal and hexagonal phases of MnFeAs. Total, Mn and Fe DOS contributions are marked by solid, dotted and dashed lines, respectively (E_F is placed at zero).

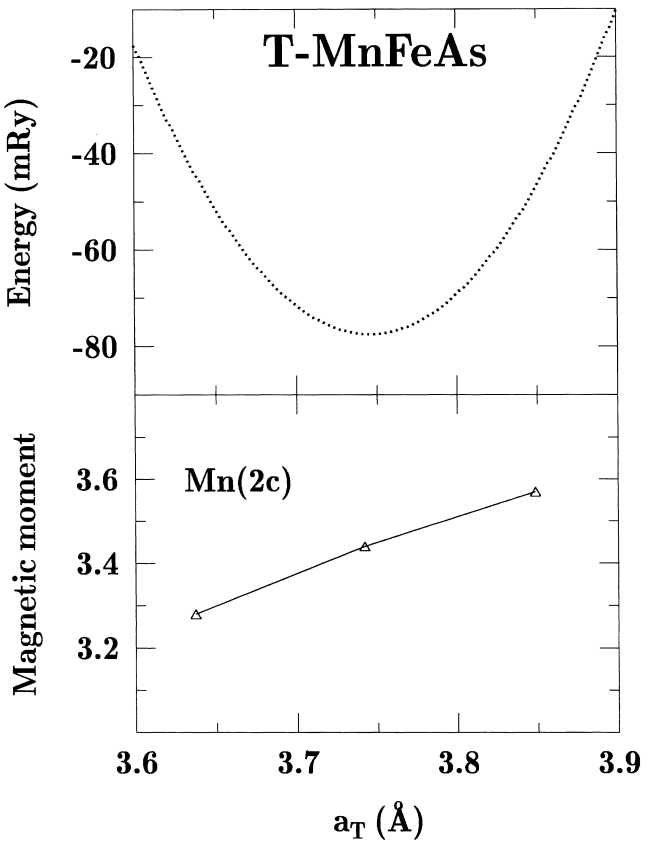

Fig. 3. Total energy parabola in the T-MnFeAs derived from the spin-polarised KKR calculations (c_T=constant). Below, the Mn magnetic moment variation versus a_T.

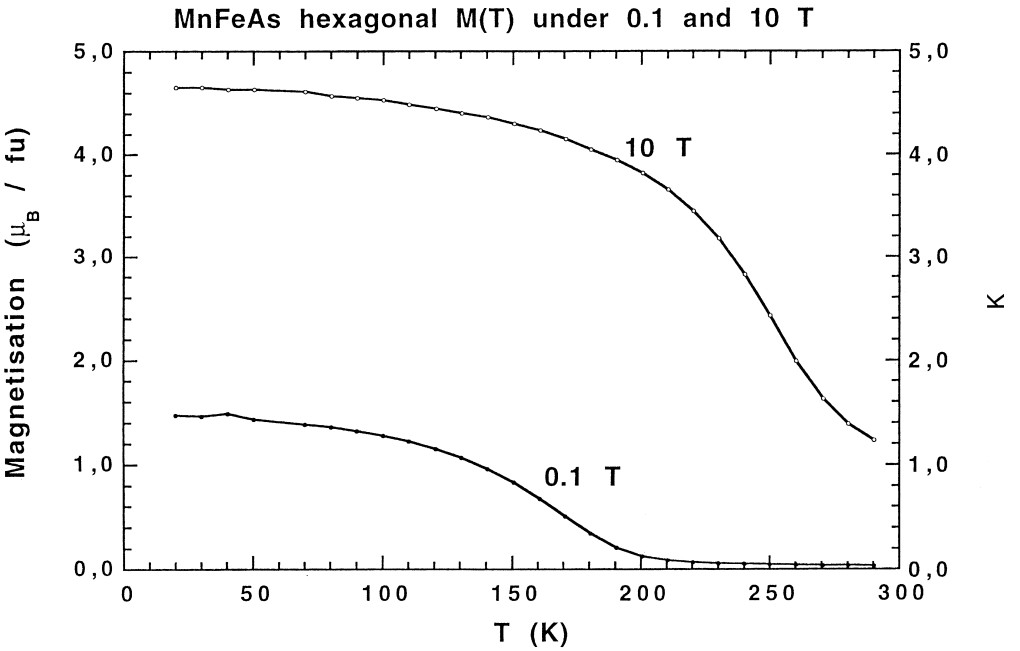

Fig. 4. Variation of magnetisation with temperature at different fields in H-MnFeAs.

system is increased in the H-type structure due to two large d-like peaks located slightly below E_F instead of one peak observed in the T phase. In more complete analysis of a structural stability, the spin-polarisation as well as all contributions to E_{tot} (not only the band term) should be taken into account. The spin-polarised total energy KKR computations on the tetragonal MnFeAs were performed for various a_T (assuming c_T = constant). In this approach the calculated equilibrium volume of T-MnFeAs derived from the total energy parabola (Fig. 3) remains in remarkable agreement with the experimental value at 5 K (V_{exp} = 83.981 Å^3, V_{th} = 84.31 Å^3). On the other hand, the H-MnFeAs compound requires a more complex analysis of the total energy depending on several variables $E_{tot}(a_H, c_H, x_{Mn}, x_{Fe})$. This analysis is not presented here.

Isofield $M_T(B)$ magnetisation measurements were carried out on the H-MnFeAs compound and the results are shown in Fig. 4. The $M_T(B)$ curve in a magnetic field of B = 0.1 T exposed that the magnetisation saturation cannot be completely reached, probably due to magnetic anisotropy. The Curie temperature was determined to be near 190 K. When applying a magnetic field as large as 10 T, the extrapolated saturation at 6 K was found to be 4.5 μ_B/f.u. (Fig. 5). The refinement of neutron diffraction data in the hexagonal type of MnFeAs led to the c-axis ferromagnetic arrangement with 3.14 μ_B on Mn(3g) and

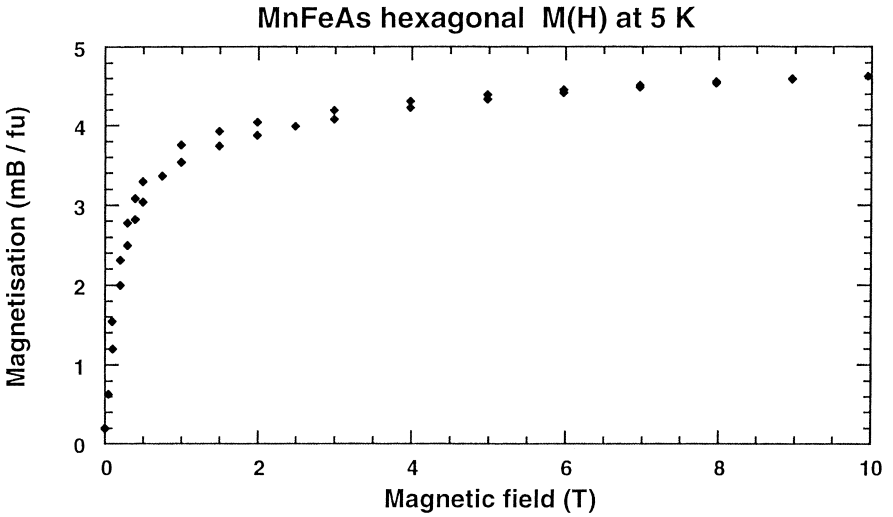

Fig. 5. Variation of magnetisation versus applied magnetic field at different temperatures in H-MnFeAs.

1.54 μ_B on Fe(3f). Thus the total magnetisation derived from the neutron experiment agrees rather well with the corresponding value obtained from the magnetisation measurement.

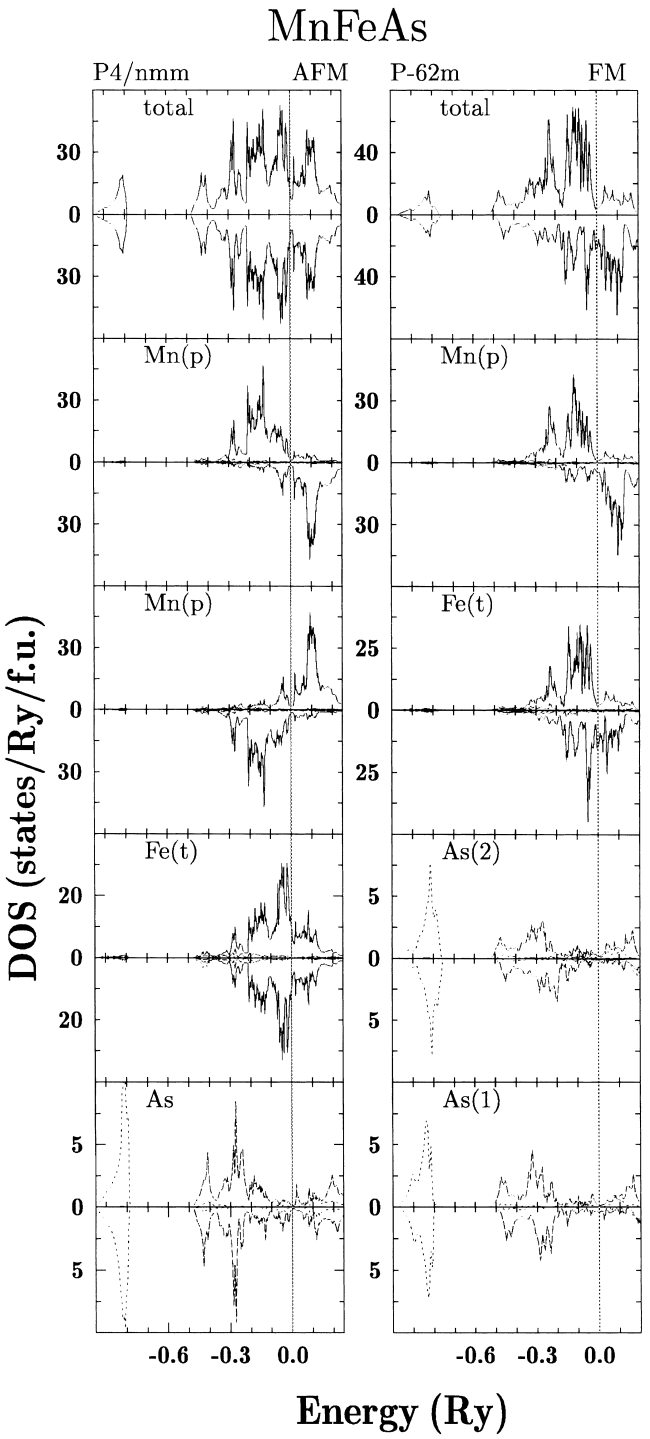

Fig. 6. Spin polarised KKR density of states in the T-MnFeAs antiferromagnet (left) and the H-MnFeAs ferromagnet (right) using experimental crystal parameters (E_F is placed at zero). s-, p- and d-DOS are depicted by dotted, dashed and solid lines, respectively. No DOS polarisation is found on Fe(t) in the tetragonal structure in contrast to Fe(t) in the hexagonal phase.

The spin-polarised computations on H-MnFeAs resulted in a distribution of electronic states as shown in Fig. 6 (right column). We observe strongly polarised conduction bands formed (below E_F) mostly from d-states on Mn and Fe, which are hybridised with p-states in As in the lower-lying energy range. The total magnetisation is due to magnetic moments 3.13 and 1.10 μ_B on Mn(3g) and Fe(3f) sites, respectively. The KKR value of μ_{Mn} remains in excellent agreement with our neutron data but the theoretical value of μ_{Fe} is rather smaller in relation to the experimental data. Note, that in the closely related Fe_2P compound, band structure calculations [5] also gave smaller value of μ_{Fe} than the experimental one on the t-site, unlike the p-site, where an agreement was fair.

From the magnetic contributions to neutron diffraction, measured in T-MnFeAs, we refined the magnetic moments of the 3.36 and 0.03 μ_B on the pyramidal Mn(2c) and tetrahedral Fe(2a), respectively. The Neél temperature was determined near 470 K. The antiferromagnetic arrangement on the Mn(2a) site is the same as Mn(p) in Mn_2As.

The KKR calculations of T-MnFeAs, assuming the above-mentioned antiferromagnetic structure, resulted in the electronic spectra as presented in Fig. 6 (left column). Interestingly, the magnetic moment on the Fe(2a) site is no more observed due to vanishing of spin polarisation seen on the Fe-DOS (Fig. 6), while that one computed on Mn(2c) is equal to 3.42 μ_B. Observing the DOS on Fe in the antiferromagnetic T-MnFeAs (Fig. 6) we conclude that the Fermi level lies on the strongly varying slope of DOS and the $N_{Fe}(E_F)$ value is near the Stoner criterion. Indeed, when making computations on T-MnFeAs in the ferromagnetic state we obtained the DOS splitting on both metal sites (not shown). Despite the computed total magnetic moment 4.0 μ_B in the ferromagnetic T-MnFeAs is rather close to the KKR value in the ferromagnetic H-MnFeAs, the distribution of the local magnetic moments, namely 0.62 μ_B on Fe and 3.44 μ_B on Mn, differ from those computed in the hexagonal phase.

Plotting the magnetic moments of Mn and Fe for both MnFeAs structures versus the mean ⟨M–M⟩ distance, we observed that experimental (also theoretical) data follows more or less a straight line (Fig. 7). However, our conclusion should be taken with care, as the preliminary KKR calculations showed that an appearance of a small magnetic moment on Fe seems to be very sensitive to the type of considered magnetic structure.

4. Conclusions

The magnetisation and neutron diffraction measurements on the tetragonal and hexagonal MnFeAs reveal that T-MnFeAs is an antiferromagnet (T_N=470 K) supported only by local magnetic moment on Mn(2c), which are arranged as in Mn_2As on the pyramidal site, while H-MnFeAs is a *c*-axis ferromagnet (T_C~190 K) with a net

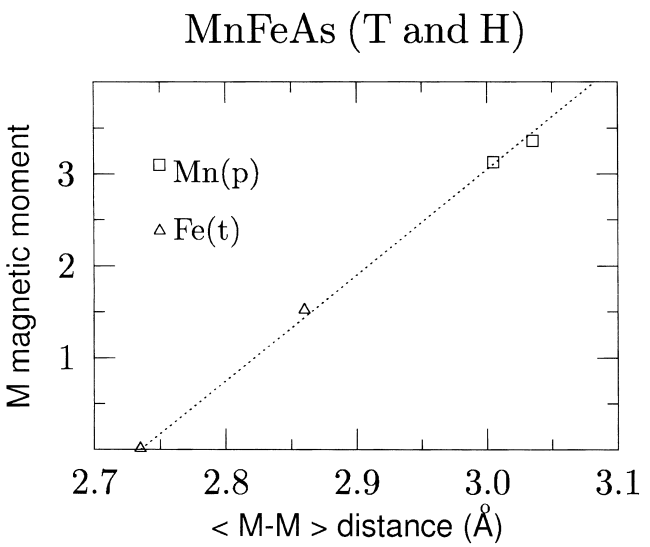

Fig. 7. Experimental magnetic moments in the tetragonal and hexagonal MnFeAs versus mean ⟨M–M⟩ distance.

magnetisation near 4.5 μ_B/f.u. (under a field of 10 T) and magnetic moments both on Mn (3.14 μ_B) and Fe (1.54 μ_B). Slight differences between magnetisation and neutron diffraction data should come from not completely saturated $M_B(T)$ curves (at 10 T), which may indicate non-ferromagnetic components in the H-MnFeAs phase.

The KKR band structure calculations performed on the tetragonal and hexagonal structures of MnFeAs (using experimental crystallographic parameters) gave a deep minimum of non-polarised DOS in the vicinity of E_F. It may tentatively explain the structural stability of both phases. The spin-polarised computations emerge that the magnetic behaviours in the T-MnFeAs antiferromagnet are related exclusively to the local moments on the Mn(2c) site (3.42 μ_B), while in the H-MnFeAs ferromagnet, total magnetic moment is distributed between Mn(3g) 3.13 μ_B and Fe(3f) 1.10 μ_B. In Table 2 the experimental and theoretical results are compared, showing a fair agreement between the magnetic measurements and the KKR computations.

Table 2
Magnetic properties (in μ_B) in the tetragonal (AFM) and hexagonal (FM) phases of MnFeAs[a]

	T-MnFeAs		H-MnFeAs	
	Experiment	Theory	Experiment	Theory
M_{tot}	0.0	0.0	4.5	4.20
μ_{Mn}	3.36	3.42	3.14	3.13
μ_{Fe}	0.03	0.01	1.54	1.10

[a] Comparison between the magnetisation, neutron diffraction measurements and the KKR band structure results.

References

[1] A. Krumbugel-Nylund, Ph.D. Thesis, University of Orsay, 1974.
[2] R. Zach, M. Guillot, R. Fruchart, J. Magn. Magn. Mater. 89 (1990) 221.
[3] M. Bacmann, J.L. Soubeyroux, R. Barett, D. Fruchart, R. Zach, S. Niziol, R. Fruchart, Magn. Magn. Mater. 134 (1994) 59.
[4] B. Malaman, G. Le Caer, P. Delcroix, D. Fruchart, R. Zach, S. Niziol, R. Fruchart, Phys.: Condens. Matter 8 (1996) 8653.
[5] J. Tobola, M. Bacmann, D. Fruchart, S. Kaprzyk, A. Koumina, S. Niziol, J.L. Soubeyroux, P. Wolfers, R. Zach, J. Magn. Magn. Mater. 157/158 (1996) 708.
[6] R. Fruchart, Ann. Chim. Fr. 7 (1982) 563.
[7] L. Hollan, Ann. Chim. 1 (1966) 437.
[8] A. Koumina, M. Bacmann, D.R. Fruchart, M. Fruchart, J. Mesnaoui, P. Tobola, P. Wolfers, in: Proceedings of the REMCES VIII Conference, Tetouan, 27–29 October, 1999.
[9] S. Yoshii, H. Katsuraki, J. Phys. Soc. Jpn. 21 (1966) 205.
[10] S. Yoshii, H. Katsuraki, J. Phys. Soc. Jpn. 22 (1967) 674.
[11] A.E. Austin, E. Adelson, W.H. Cloud, J. Appl. Phys. 33 (1962) 1356.
[12] N.N. Sirota, V.M. Ryshkovskii, Sov. Phys. – Solid State 16 (1975) 1714.
[13] H. Katsuraki, K. Suzuki, J. Appl. Phys. 36 (1965) 1094.
[14] S. Kaprzyk, Acta Phys. Pol. A 91 (1997) 135.
[15] A. Bansil, S. Kaprzyk, P.E. Mijnarends, J. Tobola, Phys. Rev. B 60 (1999) 13396.
[16] P. Wolfers, J. Appl. Cryst. 23 (1990) 554.
[17] A. Antoniadis, J. Berruyer, A. Filhol, Internal Report, ILL, 1987, 87AN20T.
[18] U. von Barth, L. Hedin, J. Phys. C 5 (1972) 1629.